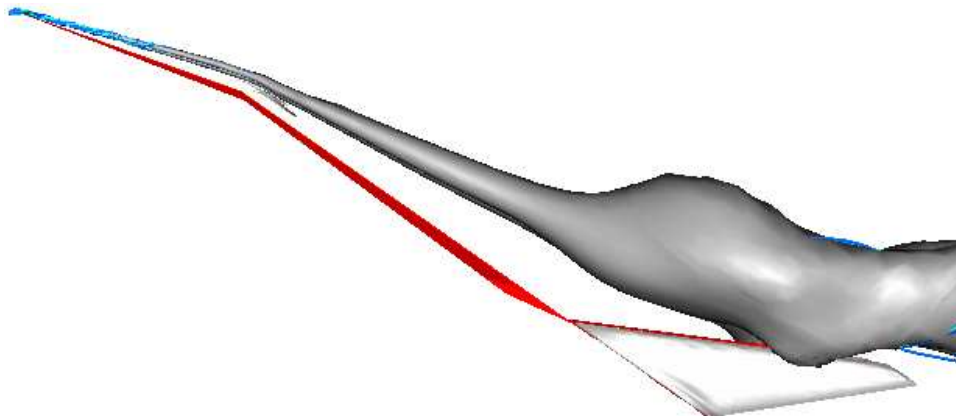


AIAA 98-0762

Effect of Apex Flap Deflection on Vertical Tail Buffeting

Steven J. Massey and Osama. A. Kandil
Old Dominion University, Norfolk, VA 23529-0247



**36th AIAA Aerospace Sciences
Meeting and Exhibit**
January 12–15, 1998 / Reno, NV

Effect of Apex Flap Deflection on Vertical Tail Buffeting

Steven J. Massey* and Osama. A. Kandil†
Old Dominion University, Norfolk, VA 23529-0247

A computational study of the effect of vortex breakdown location on vertical tail buffeting is conducted. The position of the breakdown is modified by employing an apex flap deflected by an experimentally determined optimal angle. The delayed breakdown flow and buffeting response is then compared to the nominal undeflected case. This multidisciplinary problem is solved sequentially for the fluid flow, the elastic tail deformations and the grid displacements. The fluid flow is simulated by time accurately solving the unsteady, compressible, Reynolds-averaged Navier-Stokes equations using an implicit, upwind, flux-difference splitting finite volume scheme. The elastic vibrations of the tails are modeled by uncoupled bending and torsion beam equations. These equations are solved accurately in time using the Galerkin method and a five-stage Runge-Kutta-Verner scheme. The grid for the fluid dynamics calculations is continuously deformed using interpolation functions to disperse the displacements smoothly throughout the computational domain. An angle-of-attack of 35° is chosen such that the wing primary-vortex cores experience vortex breakdown and the resulting turbulent wake flow impinges on the vertical tails. The dimensions and material properties of the vertical tails are chosen such that the deflections are large enough to insure interaction with the flow, and the natural frequencies are high enough to facilitate a practical computational solution. Results are presented for a baseline uncontrolled buffeting case and a delayed breakdown case in which the apex flap has been deflected 15° . The flap was found to be very effective in delaying the breakdown, increasing the location from 50%c to 94%c, which resulted in a 6% increase in lift coefficient and pitching moment. However, the integrated buffet loads and tip responses were roughly equivalent for the two cases.

Nomenclature

a	local speed of sound	L	vertical tail length
\vec{a}_t	absolute acceleration of the tail	M	integrated moment per unit length on tail, structural mass matrix, Mach number
b	beam width	M_{RB}	root bending moment
C_M	moment per unit length, $\frac{M}{q_\infty S_t}$	M_{RT}	root twisting moment
C_N	force per unit length, $\frac{N}{q_\infty \bar{c}}$	m	mass per unit length
C_p	coefficient of pressure, $\frac{p}{q_\infty}$	N	integrated force per unit length on tail
C_{RBM}	coefficient of root bending moment, $\frac{M_{RB}}{q_\infty S_t \bar{c}}$	n	reduced frequency, $\frac{f \bar{c}}{U_\infty}$
C_{RTM}	coefficient of root twisting moment, $\frac{M_{RT}}{q_\infty S_t \bar{c}}$	p	nondimensional pressure, $\frac{\bar{p}}{q_\infty}$
c	wing root chord	p_0	nondimensional total pressure, $\frac{\bar{p}_0}{\rho_\infty \bar{a}_\infty^2}$
\bar{c}	mean wing aerodynamic chord	Q	generalized aerodynamic force vector
d	beam thickness	$q(t)$	generalized structural coordinate
E	modulus of elasticity	q_∞	freestream dynamic pressure, $\frac{1}{2} \rho_\infty U_\infty^2$
\vec{E}_m	inviscid flux vector	\vec{Q}	vector of conserved flow variables
$(\vec{E}_v)_m$	viscous flux vector	Re	root chord Reynolds number, $\frac{\rho U c}{\mu}$
e_t	total energy per unit mass	S_t	tail plan area
f	frequency	s_1	wing semispan
G	modulus of rigidity	τ	nondimensional time, $\frac{t U_\infty}{\bar{c}}$
I	area moment of inertia	\vec{V}	velocity vector
I_{zzCM}	mass moment of inertia about the tail span axis	w	bending deflection of tail
I_θ	mass moment of inertia about the elastic axis	x_θ	distance between the elastic and inertial axes
J	polar moment of inertia, coordinate Jacobian	α	angle-of-attack
K	structural stiffness matrix	β	apex flap deflection angle
		θ	angle of twisting displacement
		ϕ	free vibration modes for bending and torsion

*Currently a Scientist at Analytical Services & Materials, Inc., Edwards, CA, Member AIAA.

†Professor, Eminent Scholar and Chair of the Department of Aerospace Engineering, Associate Fellow AIAA.

Copyright ©1998 by Osama. A. Kandil. Published by the American Institute of Aeronautics and Astronautics, Inc. with permission.



Fig. 1 F-18 HARV smoke and tuft flow visualization, $\alpha = 20^\circ$. NASA Dryden photo EC89-0096-206.

Introduction

VERTICAL tail buffeting has become an important issue with the advent of supermaneuverable aircraft capable of sustained flight at very high angles-of-attack, such as the F-18 HARV, shown in Figure 1. Unfortunately, at high angles-of-attack the vortices which support the aircraft burst forward of the tails immersing them in a wake of highly unsteady, swirling flow. This flow results in severe buffeting of the tails and has led to their premature fatigue failure. Because the burst vortex is considerably weaker, it is desirable to delay vortex breakdown as long as possible to achieve maximum high angle-of-attack capability. However, the effect on tail buffeting must also be considered, which is the subject of this paper.

In the past decade, tail buffet has been the subject of substantial experimental inquiry. In 1989, Fisher, Del Frate and Richwine¹ conducted flight test on the NASA F/A-18 High Alpha Research Vehicle (HARV). Flow visualizations revealed extensive regions of separated, reversed, and vortical flow on the wing at angles-of-attack above 20° .

More recently, Moses and Pendleton,² compared tail pressure measurements between full-scale and 1/6-scale models. Results were presented in terms of non-dimensional buffet excitation parameter and power spectral densities of root bending moment for an angle-of-attack range of 7° to 40° and Mach and Reynolds numbers up to 0.15 and 12.3×10^6 , respectively. The LEX fence was confirmed to be effective at reducing buffet loads for $\alpha < 32^\circ$. It was found that the data trends for the two different size models scaled well using a simple scaling equation.

An experimental investigation of vortex breakdown induced tail buffeting, particularly relevant to this study, is that of Washburn, Jenkins and Ferman.³ They conducted an extensive investigation into vortex-tail interaction using a 76° delta wing with twin ver-

tical tails. The vertical tails were placed at nine locations aft of the delta wing. The results showed that the aerodynamic loads were more sensitive to the chord-wise tail location than the spanwise location. The buffeting response was seen to decrease as the tails were moved towards the vortex core. It was also shown that the core trajectories upstream of the tail were not influenced by the tail location, but the breakdown location was. Additionally, the investigation showed that the presence of a flexible tail can affect the unsteady pressures on a rigid tail located on the opposite side of the model. The inboard span model of the Washburn et al.³ study is the basis of the present numerical study.

In 1990, Edwards⁴ assessed the computational cost of direct numerical simulation of tail buffeting. He concluded that computer speed would have to increase by a factor of a thousand before full aircraft computations would become practical, thus reducing a 1000-hour computation to only 1 hour. His time estimates were based on 40μ seconds per grid cell per time step for thin-layer Navier Stokes solutions. The current run time for the full Navier-Stokes equations on a single processor of a Cray C90 is 7.8μ seconds per grid cell per time step, a factor of only five times faster. Because of this high computational cost, very few numerical studies have been conducted to date⁵⁻¹⁹ and of those, the *only* ones to include aeroelastic effects are those by the author's research group,¹¹⁻¹⁹ led by O.A. Kandil.

In 1992, Rizk et al.^{5,6} investigated the unsteady loads on vertical tails by solving the Reynolds-averaged Navier-Stokes equations time accurately for a F/A-18 at $\alpha = 30^\circ$. The flow field and response were qualitatively similar to some experimentally observed phenomena. To model the symmetric half of the aircraft, a Chimera-type grid consisting of 0.9 million cells was used. Note that, in studies conducted by Kandil, Massey and Kandil,¹⁴ the same number of grid points were used to resolve the flow about a simple delta wing. In a later study by the same group,⁷ a refined grid consisting of 1.7 million cells produced significantly better results for aerodynamic loads. Another issue with the Rizk et al.^{5,6} studies is "weak coupling" between the aerodynamics and the structures. The flow only saw a fixed, rigid tail. Thus, all of the inertial effects on the local flow field from the very high accelerations of the tail were neglected. Moreover, their model neglected the aerodynamic damping originating from the interaction between the deflected tail and the flow. These effects have been shown, experimentally^{3,20} and computationally,¹¹ to significantly affect the unsteady pressure loading on the tails. Although, this latter concern can be easily alleviated by the implementation of moving grids, the high computational cost of accurately solving for a full aircraft configuration remains.

In 1993, Kandil, Kandil and Massey¹¹ solved the three-dimensional, unsteady, compressible, Navier-Stokes equations time accurately on the single tail/delta wing configuration. The tail was modeled as a cantilevered beam in bending only and was fully coupled with the aerodynamics. Variations in tail size, location, and structural properties were investigated. The solutions showed that the tail location, shape, flexibility and motion affect the upstream flow field.

In 1996, twin vertical tail buffeting was successfully simulated. Kandil, Sheta and Massey¹⁸ considered twin vertical F/A-18 tails mounted behind a 76° delta wing. Also in 1996, Kandil, Massey and Sheta¹⁹ simulated the experimental setup of Washburn et al.³ Early results were found to be in full qualitative agreement with the experimental data. A complete analysis of this case is included in the first author's dissertation.²¹ The Washburn et al.³ experimental study was first published with a companion numerical study by Krist et al.⁸ Unfortunately the choice of a low angle-of-attack and Mach number produced *no vortex breakdown whatsoever*, and therefore no buffet loads. Very recently a numerical simulation of the same configuration was also conducted by Findlay.⁹ Although, the flow parameters were sufficient to produce the buffeting breakdown flow, no attempt was made to predict or include aeroelastic effects into Findlay's simulation.

There are essentially two methods of attacking the problem of control of vortex breakdown induced tail buffeting in the flow regime: removing the vortex breakdown while preserving the vortex itself; or diffusing the vortex at some location upstream of the tails so as to optimize the balance between the benefit of vortex lift and the adverse effects of the post breakdown buffeting flow. Perhaps because of the difficulty of preventing breakdown in the presence of vertical tails, the method of choice for the F/A-18 has been diffusion.

Through trial and error the F/A-18 was retro-fitted with a short fence normal to the surface of the LEX, see Figure 2, in order to diffuse the vortex strength while having a minimal effect on aircraft aerodynamics, Lee and Valerio.²² In flight tests by Lee et al.²³ without the LEX fence, peak accelerations of $450g$ close to the tip of the vertical tail were measured. With the addition of LEX fences, the peak accelerations were reduced to $200g$. While this solution provides significant buffet relief, diffusion does impose an aerodynamic penalty and is less effective at high angles-of-attack.²⁴⁻²⁶

Recalling the fact that buffeting is a structural problem at its core, another avenue of attack is the control of the tail itself. This can be accomplished in several ways; engineering a structure or material that is less susceptible to fatigue, using composites to create a strain hardening tail, or active structural control using piezoelectric panels for active stiffening. Although, the first two methods are simpler in the long run, initial

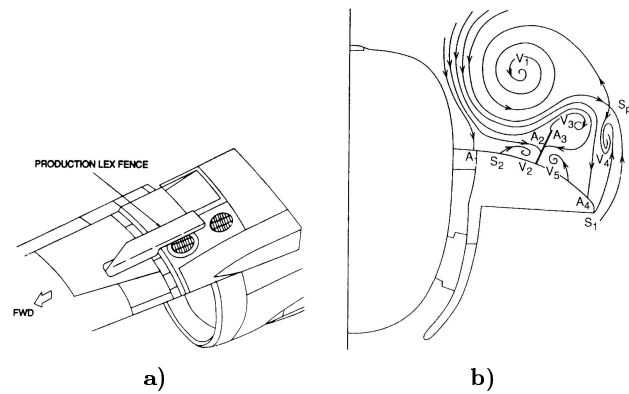


Fig. 2 LEX fence shown a) installed and with b) front view flow field topology sketched. Lee and Valerio²²

test of active buffet damping through the use of piezoelectrics have produced favorable results, e.g., Hauch et al.²⁷

In the present study, the effectiveness of an apex flap on the reduction of tail buffeting is considered for the inboard span tail case of Washburn et al.³ The inboard span case was selected because it exhibited the highest overall buffeting of the three spanwise tail positions. The apex flap was hinged at the 40% chord station and is deflected using a single optimum angle of 15° which was determined experimentally by Klute et al.²⁸ for a 76° delta wing without tails. Klute et al.²⁸ found the apex flap to be the most efficient way to delay vortex breakdown on a delta wing. The current study seeks to determine the effect this has on tail buffeting.

Formulation

In this study, two sets of governing equations, along with certain initial and boundary conditions, are used to formulate the problem of vortex breakdown induced vertical tail buffeting. The first set is the laminar, unsteady, compressible Navier-Stokes equations. The second set consist of elastic beam equations for inertially coupled bending and torsion vibrations. The grid for the fluid dynamics calculations is continuously deformed using algebraic interpolation functions to disperse the displacements smoothly throughout the computational domain.

Fluid Dynamics

For complex flow fields with strong viscous-inviscid interactions, reduced forms of the equations of fluid motion do not provide an adequate model of the flow physics. In the present study, strong viscous-inviscid interactions in the form of large-scale three-dimensional boundary-layer separation require that the full Navier-Stokes equations be considered. The conservative form of the dimensionless, unsteady, compressible, Navier-Stokes equations in time-dependent,

body-conformed coordinates, $\xi^m(x_1, x_2, x_3, t)$ is

$$\frac{\partial \bar{Q}}{\partial t} + \frac{\partial}{\partial \xi^m} [\bar{E}_m - (\bar{E}_v)_m] = 0 \quad (1)$$

where the flow state, inviscid flux and viscous flux vectors are as follows,

$$\bar{Q} = \frac{1}{J} \begin{Bmatrix} \rho \\ \rho u_1 \\ \rho u_2 \\ \rho u_3 \\ \rho e_t \end{Bmatrix} \quad (2)$$

$$\bar{E}_m = \frac{1}{J} \begin{Bmatrix} \rho U_m \\ \rho u_1 U_m + \frac{\partial \xi^m}{\partial x_1} p \\ \rho u_2 U_m + \frac{\partial \xi^m}{\partial x_2} p \\ \rho u_3 U_m + \frac{\partial \xi^m}{\partial x_3} p \\ U_m (\rho e_t + p) - \frac{\partial \xi^m}{\partial t} p \end{Bmatrix} \quad (3)$$

$$(\bar{E}_v)_m = \frac{1}{J} \begin{Bmatrix} 0 \\ \frac{\partial \xi^m}{\partial x_k} \tau_{1k} \\ \frac{\partial \xi^m}{\partial x_k} \tau_{2k} \\ \frac{\partial \xi^m}{\partial x_k} \tau_{3k} \\ \frac{\partial \xi^m}{\partial x_k} (u_i \tau_{ik} - q_k) \end{Bmatrix} \quad (4)$$

The contravariant velocity component (U_m) in the ξ^m direction in Eq.(3) is

$$U_m = \frac{\partial \xi^m}{\partial t} + \frac{\partial \xi^m}{\partial x_k} u_k \quad (5)$$

and the shear stress and heat conduction components in Eq.(4) are given by

$$\tau_{ik} = \frac{\mu M_\infty}{Re_\infty} \left(\frac{\partial \xi^m}{\partial x_k} \frac{\partial u_i}{\partial \xi^m} + \frac{\partial \xi^m}{\partial x_i} \frac{\partial u_k}{\partial \xi^m} - \frac{2}{3} \delta_{ik} \frac{\partial \xi^m}{\partial x_j} \frac{\partial u_j}{\partial \xi^m} \right) \quad (6)$$

and

$$q_k = -\frac{\mu M_\infty}{Re_\infty Pr(\gamma - 1)} \frac{\partial \xi^m}{\partial x_k} \frac{\partial a^2}{\partial \xi^m} \quad (7)$$

where a is the dimensionless local speed of sound and $a^2 = T$.

Structural Dynamics

Each tail is modeled as a cantilevered beam capable of bending and twisting. The formulation allows for inertial coupling of the bending and torsion modes due to separation of the inertial and elastic axes by a distance of x_θ . In the present study, the bending and torsion vibrations are uncoupled ($x_\theta = 0$). The dimensionless, linearized governing equations for the

bending (w) and torsion (θ) vibrations along the tail (z) are

$$\frac{\partial^2}{\partial z^2} \left[EI(z) \frac{\partial^2 w(z, t)}{\partial z^2} \right] + m(z) \frac{\partial^2 w(z, t)}{\partial t^2} + m(z) x_\theta(z) \frac{\partial^2 \theta(z, t)}{\partial t^2} = N(z, t) \quad (8)$$

$$\frac{\partial}{\partial z} \left[GJ(z) \frac{\partial \theta(z, t)}{\partial z} \right] - m(z) x_\theta(z) \frac{\partial^2 w(z, t)}{\partial t^2} - I_\theta(z) \frac{\partial^2 \theta(z, t)}{\partial t^2} = -M(z, t) \quad (9)$$

Eqs. (8) and (9) are solved approximately using the Galerkin method with six bending modes and six torsion modes. This method expands the dependent variables in terms of natural free vibration modes of the system. The resulting error is minimized by weighting these modes such that the error integrated over the domain is zero. The dependent variables are given by

$$w(z, t) = \sum_{i=1}^6 q_i(t) \phi_i(z) \quad (10)$$

$$\theta(z, t) = \sum_{j=7}^{12} q_j(t) \phi_j(z) \quad (11)$$

where q_i and q_j are generalized coordinates for bending and torsion, respectively, and ϕ_i and ϕ_j are comparison functions satisfying the free vibration modes of a beam in bending and torsion, respectively.

Substituting Eqs. (10) and (11) into Eqs. (8) and (9) and applying the Galerkin method and integration by parts with boundary conditions, yields the following partitioned matrix equation in generalized coordinates,

$$\begin{bmatrix} M_{11} & M_{12} \\ M_{21} & M_{22} \end{bmatrix} \begin{Bmatrix} \ddot{q}_i \\ \ddot{q}_j \end{Bmatrix} + \begin{bmatrix} K_{11} & 0 \\ 0 & K_{22} \end{bmatrix} \begin{Bmatrix} q_i \\ q_j \end{Bmatrix} = \begin{Bmatrix} Q_1 \\ Q_2 \end{Bmatrix} \quad (12)$$

where the elements of the mass matrix are

$$\begin{aligned} M_{11} &= \int_0^L m \phi_r \phi_i dz & M_{12} &= \int_0^L m x_\theta \phi_r \phi_j dz \\ M_{21} &= \int_0^L m x_\theta \phi_s \phi_i dz & M_{22} &= \int_0^L I_\theta \phi_s \phi_j dz \end{aligned} \quad (13)$$

the stiffness elements are

$$K_{11} = \int_0^L EI \frac{d^2 \phi_r}{dz^2} \frac{d^2 \phi_i}{dz^2} dz \quad K_{22} = \int_0^L GJ \frac{d\phi_s}{dz} \frac{d\phi_j}{dz} dz \quad (14)$$

and the generalized force elements are

$$Q_1 = \int_0^L N \phi_r dz \quad Q_2 = \int_0^L M \phi_s dz \quad (15)$$

The original governing equations have now been transformed from a set of two coupled partial differential equations into a set of twelve coupled second-order ordinary differential equations. In compact matrix notation, these equations are written as

$$[M]\{\ddot{q}\} + [K]\{q\} = \{Q\} \quad (16)$$

By introduction of a new variable η , the equations may be further reduced to a set of $2J$ coupled first-order ordinary differential equations. Letting

$$\{\eta\} = [I]\{\dot{q}\} \quad (17)$$

gives

$$[M]\{\dot{\eta}\} + [K]\{q\} = \{Q\} \quad (18)$$

Writing the new system in a state-space like form gives

$$\begin{Bmatrix} \dot{\eta} \\ \dot{q} \end{Bmatrix} = \begin{bmatrix} 0 & -[M]^{-1}[K] \\ [I] & 0 \end{bmatrix} \begin{Bmatrix} \eta \\ q \end{Bmatrix} + \begin{Bmatrix} [M]^{-1}\{Q\} \\ 0 \end{Bmatrix} \quad (19)$$

This final form of the governing equations is solved using a five-stage Runge-Kutta-Verner scheme.

Boundary and Initial Conditions

The Riemann-invariant boundary conditions are enforced at the inflow and outflow boundaries of the computational domain. At the plane of geometric symmetry, periodic boundary conditions are specified. On the wing surface, no-slip and no-penetration conditions ($\vec{V} = 0$) are enforced along with zero normal pressure gradient ($\frac{\partial p}{\partial n} = 0$). On the tail surfaces, the no-slip and no-penetration conditions are enforced for the relative velocity ($\vec{V} = \vec{V}_t$). Due to the acceleration of the tails, the normal pressure gradient is $\frac{\partial p}{\partial n} = -\rho \vec{a}_t \cdot \hat{n}$, where \vec{a}_t is the acceleration on the tail and \hat{n} is the unit normal.

The boundary conditions for each tail, which is clamped at the root and free at the tip, are

$$\begin{aligned} w(0, t) &= \frac{\partial w(0, t)}{\partial z} = \frac{\partial^2 w(L, t)}{\partial z^2} \\ &= \frac{\partial}{\partial z} \left[EI(L) \frac{\partial^2 w(L, t)}{\partial z^2} \right] = 0 \end{aligned} \quad (20)$$

$$\theta(0, t) = \frac{\partial \theta(L, t)}{\partial z} = 0 \quad (21)$$

The initial flow condition is freestream flow with no-slip and no-penetration conditions on the wing and tail surfaces. The initial conditions for the tails are undeformed and still,

$$w(z, 0) = \frac{\partial w(z, 0)}{\partial t} = 0 \quad (22)$$

$$\theta(z, 0) = \frac{\partial \theta(z, 0)}{\partial t} = 0 \quad (23)$$

Multidisciplinary Solution Methodology

The first step is to solve for the flow field under conditions favorable to vortex breakdown while holding the tails rigid. After the flow sets up, the tails are allowed to move. The pressure difference across each tail is obtained and used to compute the normal forces and twisting moments per unit length. With the aerodynamic forces known, the deflections, $w_{i,j,k}$ and $\theta_{i,j,k}$, can be obtained. Next, the grid is smoothly interpolated to conform to the new position and velocity of each tail. In this step, the metric coefficients of the coordinate Jacobian matrix are updated, as well as, the grid speed, $\frac{\partial \xi^m}{\partial t}$. The cycle is now repeated for the next global time step with the current tail positions and velocities as initial conditions. The time step for the fluid dynamics calculations is generally much smaller than the structural dynamics time step. Hence, $w_{i,j,k}$ and $\theta_{i,j,k}$ need not be calculated for every global time step. However, for the sake of simplicity and because of the relatively low cost of structural calculations, the structures time step is kept in line with the fluid dynamics time step. The numerical scheme is implemented in a modified version of the NASA Langley code, CFL3D.

Wing Twin-Tail Configuration

The baseline model consist of a sharp-edged, delta wing of aspect ratio one (76°) with a triangular cross-section, see Figure 3, and twin swept vertical tails placed at distance of $y = 0.082c$ from the symmetry plane. The model is based on the inboard case of Washburn et al.³ For the apex flap case, the wing is hinged at the 40% chord station and the apex is lowered 15° . The height of the tails are $0.22c$. The vertical tails are oriented normal to the upper surface of the wing and have a centerline sweep of 53.5° . Each tail root chord is $0.35c$ with a taper ratio of 0.23. See Figure 4 for a sketch of the tail with Washburn pressure tap locations. The tails are dynamically scaled with material properties corresponding to solid balsa wood based on a wing root chord of 18 inches. The tail thickness varies linearly along its span from $0.0211c$ at the root to $0.111c$ at the midspan location. From the midspan to the tip the thickness is constant. The tail cross-section is rectangular with beveled edges of 20° . To increase the deflections, the thickness was taken to be half of the actual thickness in the structures calculations. This is roughly equivalent to the addition of horizontal cuts in the tail made on the experimental model by Washburn.

To accommodate the boundary conditions of the twin tails, a five block, C^0 continuous, O-H grid is used with a total of 458,100 cells, see Figure 5. The global grid extends $0.8c$ upstream, $3c$ radially and $3.6c$ downstream. These limits were obtained from earlier numerical experiments which showed that primary flow was insensitive to the far-field boundary conditions beyond this distance. The configuration angle-of-attack

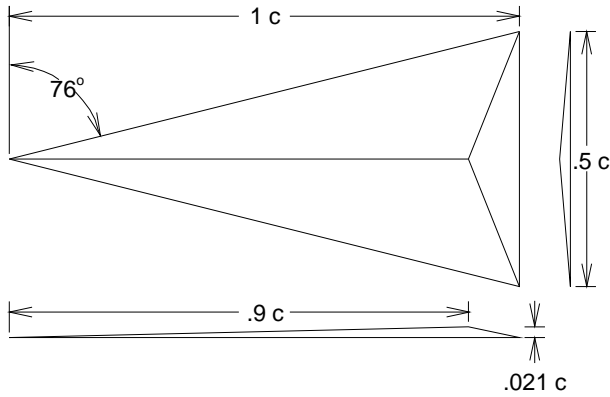


Fig. 3 Sketch of delta wing geometry.

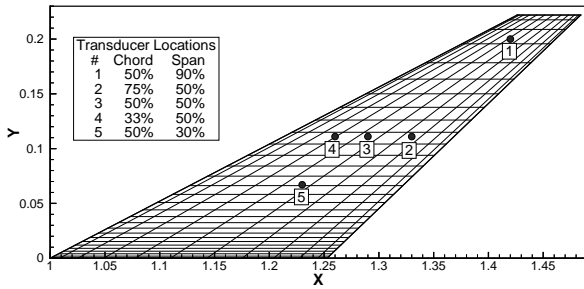


Fig. 4 Tail surface grid with Washburn pressure tap locations shown.

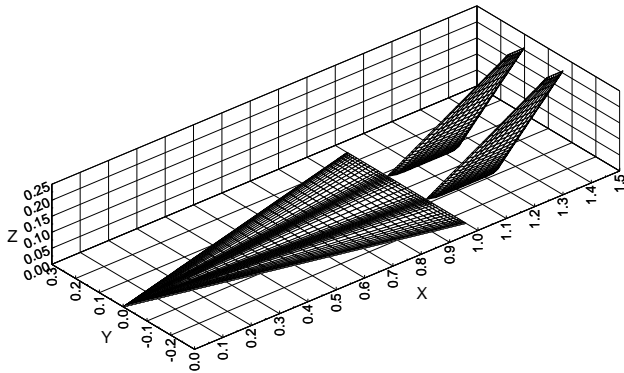


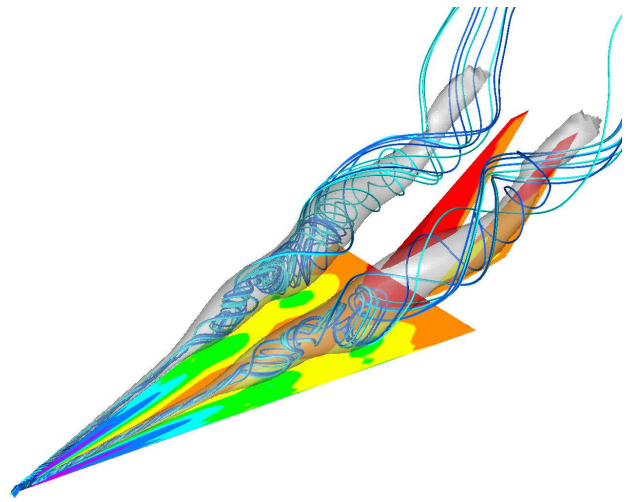
Fig. 5 Wing-twin tail configuration surface grids.

is 35° and the Mach and Reynolds numbers are 0.3 and 1.25×10^6 respectively.

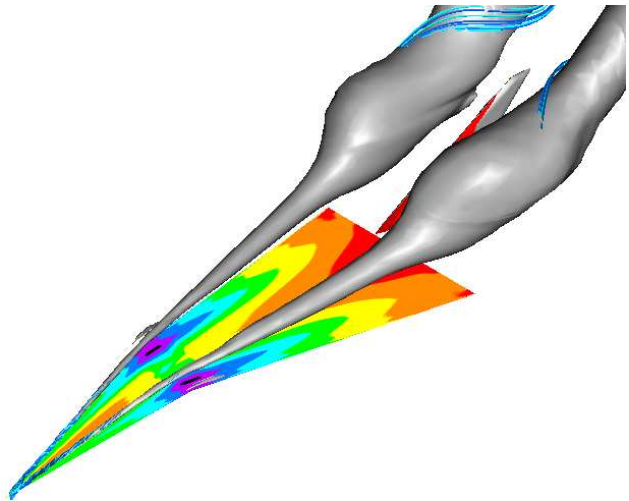
Results

Initial Conditions

The initial flow state was obtained by using local time stepping for 2000 iterations and time-accurate stepping for another five nondimensional time with $\Delta\tau = 0.00036$. Figure 6 depicts the initial flow state from which the buffeting cases are started from. For both cases the contour range and isosurface level are identical. For the baseline case, the isosurface was made transparent to reveal the internal streamlines.



a) Baseline case.



b) Deflected apex flap case.

Fig. 6 Three-dimensional views of surface pressure, vortex core streamlines and non-dimensional total pressure isosurfaces of $p_0 = 0.68$, Surface $C_p \in [-3.6, 0.8]$. Initial Condition Flowfield: $Re = 1.25 \times 10^6$, $M = 0.3$, $\alpha = 35^\circ$.

The 3D streamline and total pressure isosurface plots clearly demonstrate the effectiveness of apex flap deflection for delaying breakdown. The original burst location was 50%c and now occurs very late at 94%c. The isopressure surfaces show that the size of the breakdown has actually increased due to the flap deflection. The near surface streamlines for both cases are shown in Figures 7 and 8. The apex flap wing streamlines show a lack of curvature of the line of secondary separation on the wing, due to the aft position of the breakdown. The outer side tail surface streamlines show, that for the apex flap case, the separation line along the leading edge of the tail is much more clearly defined, indicating a stronger entrainment of fluid from the tail than in the baseline case. In Figure 9, the coefficient of pressure in the spanwise

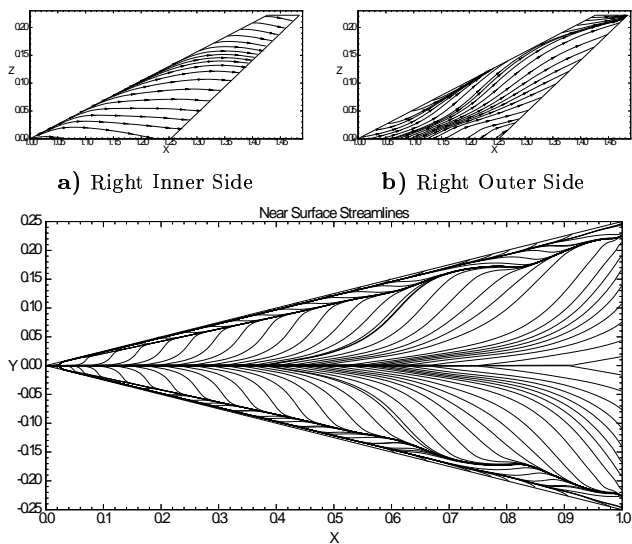


Fig. 7 Near surface streamlines for the inner and outer right tail surfaces and the upper wing surface. Undeformed Initial Condition: $\beta_{\text{Flap}} = 0^\circ$, $Re = 1.25 \times 10^6$, $M = 0.3$, $\alpha = 35^\circ$.

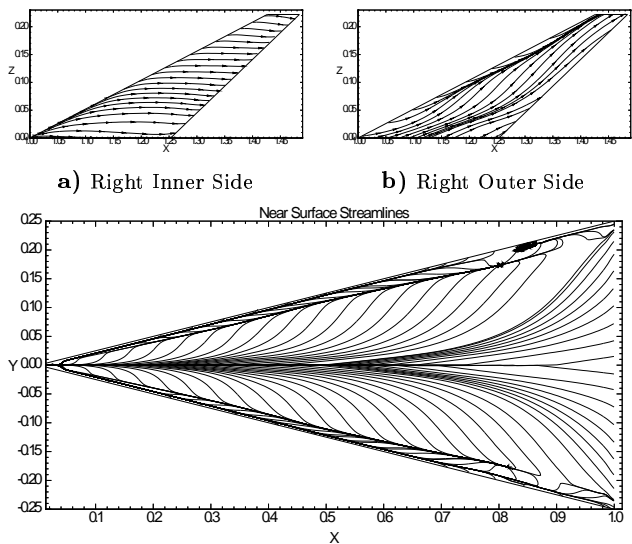


Fig. 8 Near surface streamlines for the inner and outer right tail surfaces and the upper wing surface. Deformed Initial Condition: $\beta_{\text{Flap}} = 15^\circ$, $Re = 1.25 \times 10^6$, $M = 0.3$, $\alpha = 35^\circ$.

direction show the beneficial gain in lift due to the delay of breakdown. The coefficient of lift for the apex flap case is $C_L = 1.11$ which is 6% higher than the baseline C_L of 1.05. The pitching moment coefficient also increased by 6%.

Comparison of the tail crossflow planes, shown in Figures 10 and 11, indicate that the vortices of the baseline case are generally more compact due to the smaller burst size and the greater distance upstream. The core total pressures are nearly equivalent.

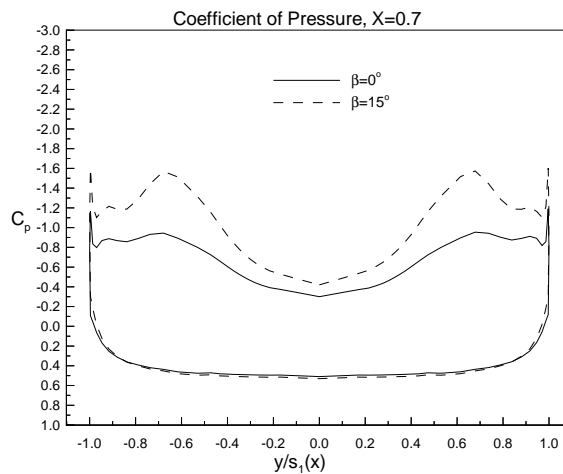
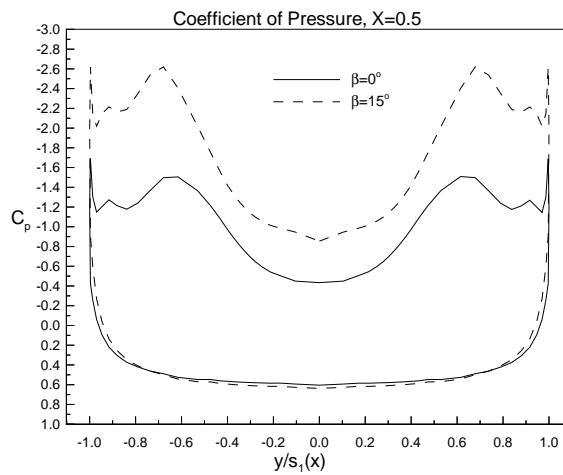
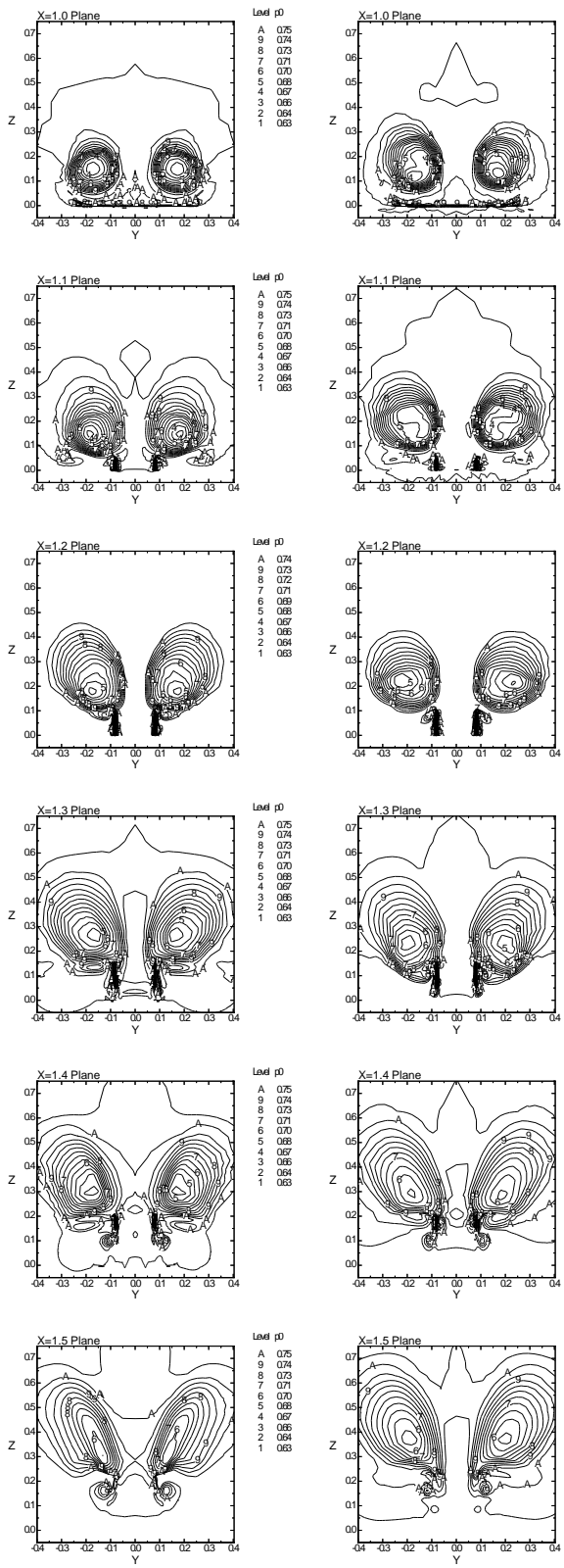


Fig. 9 Effect of apex flap deflection on wing surface coefficient of pressure. Initial Condition.

Uncoupled Bending and Torsion Response

The right tail buffet loads of the baseline and deflected apex flap cases are compared in Figures 12 - 16. The effect of the apex flap is mixed in the lumped mean and RMS loads, with the RMS moment loads showing the clearest trend of being up to 30% lower than the undeflected case. Comparison of the area mean and RMS loads, shown in Figure 13 and Figure 14 indicate that the overall levels are the same with RMS distributions exhibiting the greatest differences in their gradients.

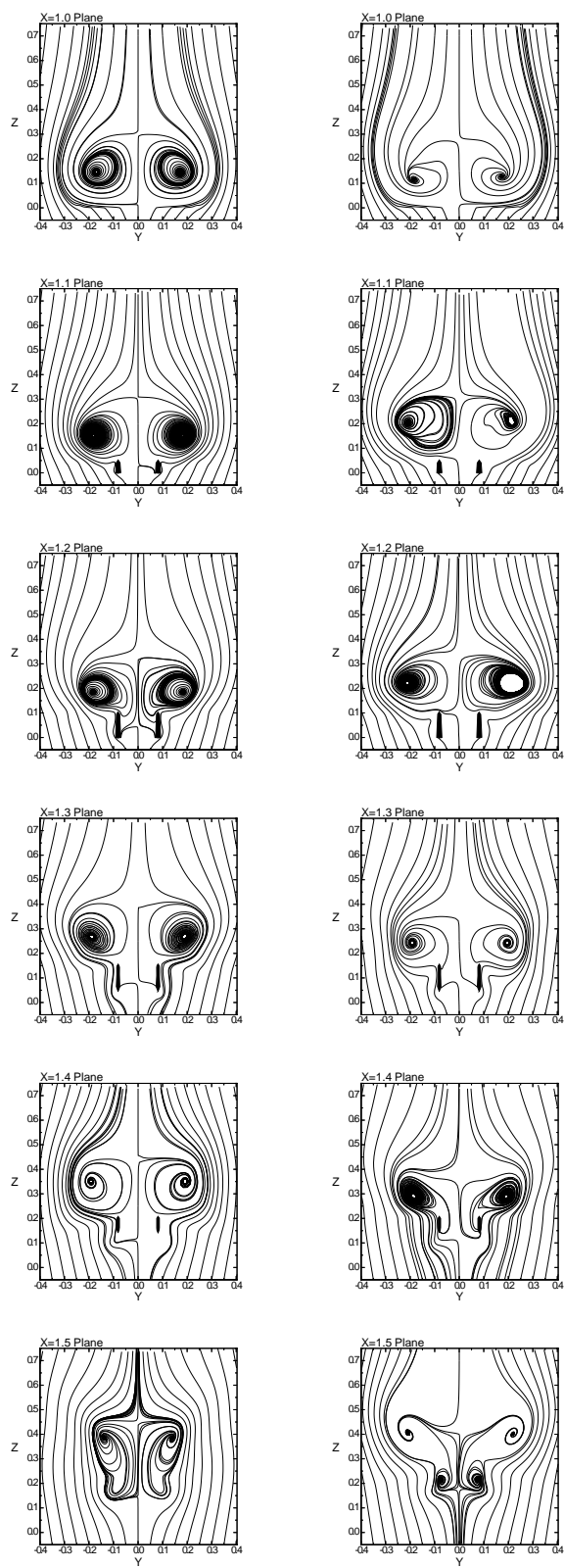
In Figure 15 the differential pressure and buffet excitation parameter at a tail chord station of 50% and tail height of 90% is plotted for both cases. The location is chosen to correspond to measurements taken by Washburn et al.³ The point buffet excitation plots show a dramatic decrease in buffeting for the apex flap case, at around 50% of the baseline case. However, this is only at one location and therefore does not necessarily represent the whole tail. Better measures of the global buffet loads are the root bending and



k) $\alpha = 0^\circ$

l) $\alpha = 15^\circ$

Fig. 10 Effect of apex flap deflection on nondimensional total pressure contours plotted on vertical crossflow planes. Initial Condition.



k) $\alpha = 0^\circ$

l) $\alpha = 15^\circ$

Fig. 11 Effect of apex flap deflection on in-plane streamlines plotted on vertical crossflow planes. Initial Condition.

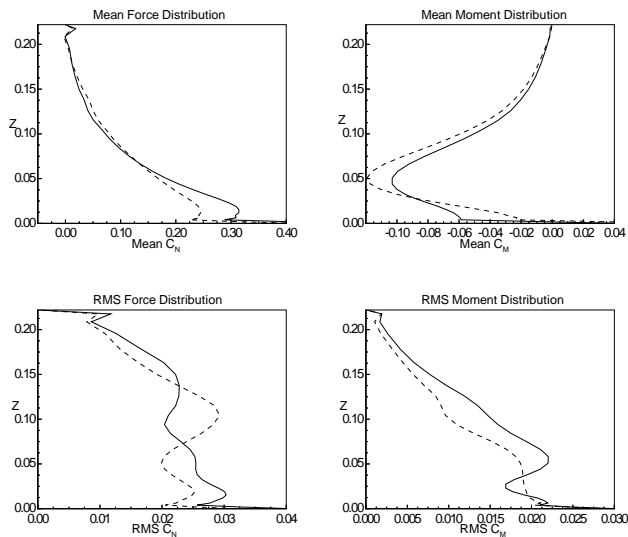


Fig. 12 Effect of apex flap on mean and RMS load distributions along the right tail span.

twisting moments, see Figure 16. These plots show that the integrated buffet levels are roughly equal between the two cases. Given the favorable change in wing loading from the apex flap, even a unchanged buffet loading is acceptable since additional wing loading may be exchanged for a lower configuration angle-of-attack which would lower the buffeting levels.

The final measure of the degree of buffeting is the response, see Figure 17. As in the root moment data, the response also indicates that there is very little change in the response due to the apex flap deflection. Hence, it is concluded that the apex flap is an efficient and harmless means of delaying vortex bursting and increasing aircraft nose authority without increasing the level of tail buffeting.

Summary

In this study, the issue of control was addressed. Results were presented for an apex flap deflection scheme which delays the onset of vortex breakdown. The configuration used was the inboard Washburn tail case which had the highest level of buffeting for all of the cases studied. The flap was deflected by a single optimum angle which was experimentally²⁸ found to produce the greatest delay in the onset of breakdown. The flap was found to be very effective in delaying the breakdown, increasing the location from 50%*c* to 94%*c*, which resulted in a 6% increase in lift coefficient over the baseline case of $C_L = 1.05$. The effect of the apex flap was mixed in the lumped mean and RMS loads, with the RMS moment loads showing the clearest trend of being up to 30% lower than the undeflected case. Comparison of the area mean and RMS loads, showed that the overall levels are the same with RMS distributions showing the greatest differences in gradients. The integrated buffet load levels are roughly equal between the two cases. Given the

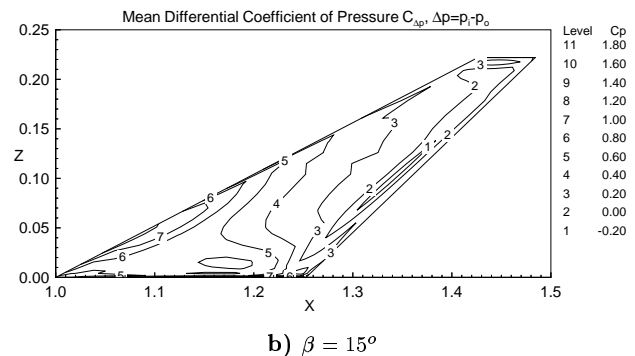
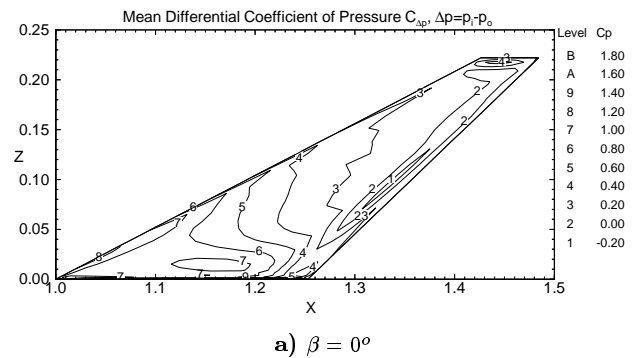


Fig. 13 Effect of apex flap on right tail mean differential coefficient of pressure contours.

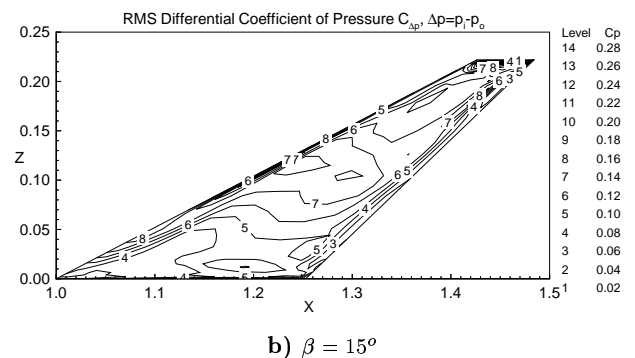
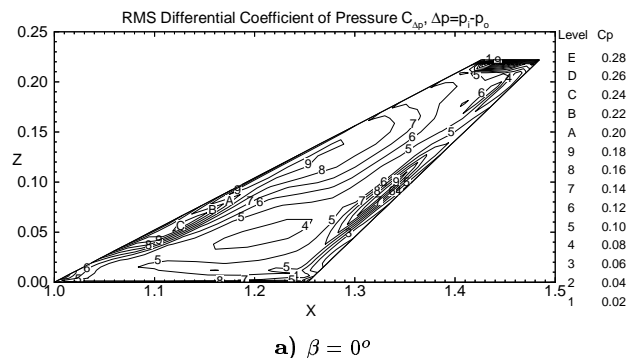


Fig. 14 Effect of apex flap on right tail RMS differential coefficient of pressure contours.

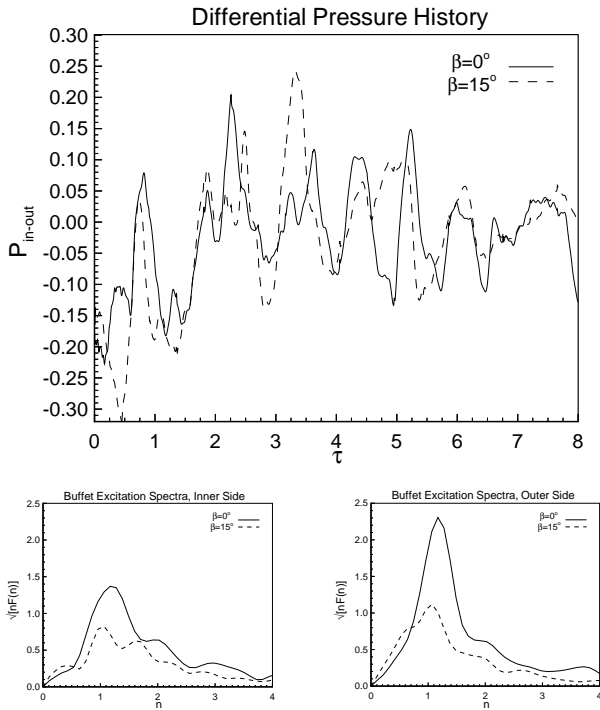


Fig. 15 Effect of apex flap on differential pressure ($\frac{\Delta p}{q_\infty}$) histories at the 50% chord and 90% span location for the right tail.

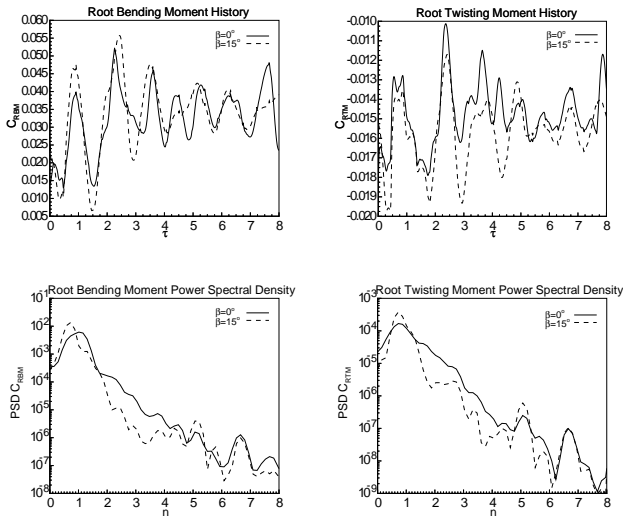


Fig. 16 Effect of apex flap on history and power spectral density of root bending moment coefficient and root twisting moment coefficient versus reduced frequency for the right tail.

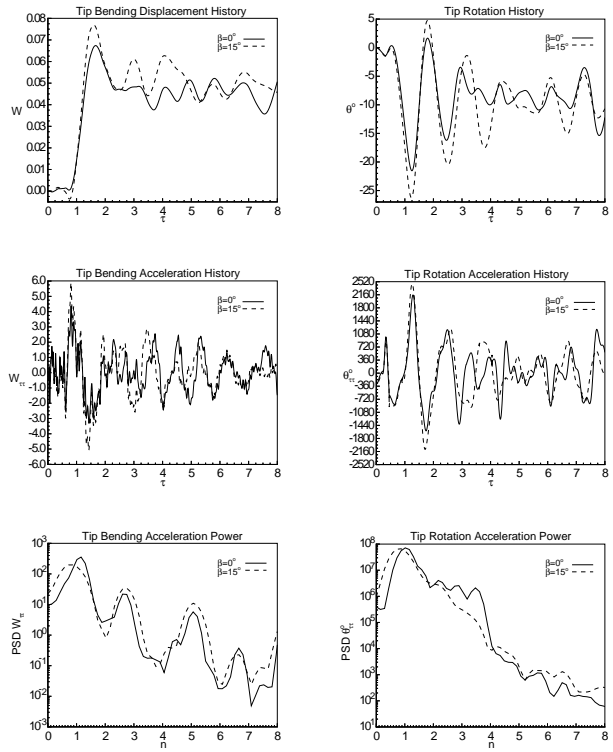


Fig. 17 Effect of apex flap on time and frequency domain data for right tail tip bending and torsion deflections and accelerations.

favorable change in wing loading from the apex flap, even an unchanged buffet loading is acceptable since additional wing loading may be exchanged for a lower configuration angle-of-attack, which would lower the buffet levels. As with in the root moment data, very little change in the response was observed due to the apex flap deflection. Hence, it is concluded that the apex flap is an efficient and harmless means of delaying vortex bursting and increasing aircraft nose authority without increasing the level of tail buffeting.

Acknowledgements

This research was supported by the Aeroelasticity Branch of NASA LaRC, under Grant No. NAG-1-648. Computational resources were provided by NASA Langley Research Center and the Numerical Aerodynamic Simulation (NAS) Program of NASA Ames Research Center.

References

- ¹Fisher, D., Del Frate, J., and Richwine, D., "In-Flight Visualization Characteristics of the NASA F-18 High Alpha Research Vehicle at High Angles of Attack," SAE 892222, September 1989.
- ²Moses, R. W. and Pendleton, E., "A Comparison of Pressure Measurements Between a Full-Scale and a 1/6-Scale F/A-18 Twin Tail During Buffet," Technical Memorandum 110282, NASA LaRC, August 1996.
- ³Washburn, A. E., Jenkins, L. N., and Ferman, M. A., "Experimental Investigation of Vortex-Fin Interaction," AIAA CP 93-0050, Jan. 1993.

- ⁴Edwards, J., "Assessment of Computational Prediction of Tail Buffeting," Technical Memorandum 101613, NASA LaRC, January 1990.
- ⁵Rizk, Y., Guruswamy, G., and Gee, K., "Numerical Investigation of Tail Buffet on F-18 Aircraft," AIAA CP 92-2673, 1992.
- ⁶Rizk, Y., Guruswamy, G., and Gee, K., "Computational Study of F-18 Vortex Induced Tail Buffet," AIAA CP 92-4699, 1992.
- ⁷Gee, K., Murman, S., and Schiff, L., "Computational Study of F-18 Vortex Induced Tail Buffet," AIAA CP 95-3440, 1995.
- ⁸Krist, S., Washburn, A., and Visser, K., "A Computational and Experimental Investigation of a Delta Wing with Vertical Tails," AIAA CP 93-3009, July 1993.
- ⁹Findlay, D., "Numerical Analysis of Vertical Tail Buffet," AIAA CP 97-0621, January 1997.
- ¹⁰Rizzetta, D., "Numerical Simulation of the Interaction between a Leading-Edge Vortex and a Vertical Tail," AIAA CP 96-2012, June 1996.
- ¹¹Kandil, O., Kandil, H., and Massey, S., "Simulation of Tail Buffet Using Delta Wing-Vertical Tail Configuration," AIAA CP 93-3688, August 1993.
- ¹²Kandil, O. and Flanagan, M., "Vertical Tail Buffet in Vortex Breakdown Flows," August 1993, In proceedings of the 5th International Symposium on Computational Fluid Dynamics, Sendai, Japan.
- ¹³Flanagan, M., *Simulation of Vertical Tail Buffet in Internal Vortex Breakdown Flows*, Master's thesis, Dept. of Aerospace Engineering, Old Dominion University, Norfolk, VA, December 1993.
- ¹⁴Kandil, O., Massey, S., and Kandil, H., "Computations of Vortex-Breakdown Induced Tail Buffet Undergoing Bending and Torsional Vibrations," AIAA CP 94-1428, 1994.
- ¹⁵Massey, S. J., *Direct Numerical Simulation of Vortex Breakdown Induced Tail Buffet*, Master's thesis, Dept. of Aerospace Engineering, Old Dominion University, Norfolk, VA, May 1994.
- ¹⁶Kandil, O., Massey, S., and Sheta, E., "Structural Dynamic / CFD Interaction for Computation of Vertical Tail Buffet," Royal Aeronautical Society Paper No 16.52, June 1995.
- ¹⁷Kandil, O., Sheta, E., and Massey, S., "Buffet Responses of a Vertical Tail in Vortex Breakdown Flows," AIAA CP 95-3464, August 1995.
- ¹⁸Kandil, O., Sheta, E., and Massey, S., "Twin Tail / Delta Wing Configuration Buffet Due to Unsteady Vortex Breakdown Flow," AIAA CP 96-2517, June 1996.
- ¹⁹Kandil, O., Massey, S., and Sheta, E., "Aerostructural Vortical Flow Interactions with Applications to F/A-18 and F-117 Tail Buffet," September 1996.
- ²⁰Triplett, W., "Pressure Measurements on Twin Vertical Tails in Buffeting Flow," *Journal of Aircraft*, Vol. 20, No. 1, 1983, pp. 920-925.
- ²¹Massey, S. J., *Development of a Coupled Fluid/Structure Aeroelastic Solver with Applications to Vortex Breakdown Induced Twin Tail Buffeting*, Ph.D. thesis, Dept. of Aerospace Engineering, Old Dominion University, Norfolk, VA <http://www.aero.odu.edu/~massey>, December 1997.
- ²²Lee, B. and Valerio, N., "Vortical Flow Structure near the F/A-18 LEX at High Incidence," *Journal of Aircraft*, Vol. 31, No. 5, 1994, pp. 1221-1223.
- ²³Lee, B., Brown, D., Zgela, M., and Poirel, D., "Wind Tunnel Investigation of Tail Buffet on the F-18 Aircraft," *AGARD Conference Proceedings No. 483, Paper 1*, 1990.
- ²⁴Meyn, L. A. and James, K. D., "Full Scale Wind Tunnel Studies of F/A-18 Tail Buffet," AIAA CP 93-3519, 1993.
- ²⁵Pettit, C. L., Brown, D., and Pendleton, E., "Wind Tunnel Test of Full-Scale F/A-18 Twin Tail Buffet: A Summary of Pressure and Response Measurements," AIAA CP 94-3476, 1994.
- ²⁶Shah, G. H., "Wind-Tunnel Investigation of Aerodynamic and Tail Buffet Characteristics of Leading-Edge Extension Modifications to the F/A-18," AIAA CP 91-2889, August 1991.
- ²⁷Hauch, R., Jacobs, J., Ravindra, K., and Dima, C., "Reduction of Vertical Tail Buffet Response Using Active Control," AIAA CP 95-1080, 1995.
- ²⁸Klute, S. M., Martin, R. A., Rediniotis, O. K., and Telionis, D. P., "Flow Control Over Delta Wings at High Angles of Attack," AIAA CP 93-3494, 1993.